# Mineral chemistry and *P-T* condition of granular and sheared peridotite xenoliths from Kimberley, South Africa: origin of the textural variation in the cratonic mantle

Ikuo Katayama[a,*], Yuka Suyama[a], Jun-ichi Ando[a], Tsuyoshi Komiya[b]

[a]*Department of Earth and Planetary Systems Science, Hiroshima University, Japan*

[b]*Department of Earth and Planetary Sciences, Tokyo Institute of Technology, Japan*

**Corresponding author:*

*Department of Earth and Planetary Systems Science, Hiroshima University, Higashi-Hiroshima 739-8526, Japan*

*Tel: +81-824-24-7468, Fax: +81-824-24-0735*

*E-mail: katayama@hiroshima-u.ac.jp*

**Abstract**

Mantle xenoliths from Kimberley, South Africa, contain texturally distinct peridotites; coarse granular to extensively sheared peridotites. Mineral chemistries of the textually distinct peridotite xenoliths indicate that these mantle rocks were equilibrated at similar *P-T* conditions: 44-54 kbar and 970-1130$^{o}$C for granular peridotites, and 41-50 kbar and 950-1080$^{o}$C for sheared peridotites. The Kimberley peridotites showing various deformation textures are restricted to a relatively narrow depth range (120-160km). They display no systematic correlation between texture and estimated equilibrium pressure and temperature, whereas sheared peridotites in the Lesotho kimberlites commonly originated from greater depths and higher temperature. The large local variations in the degree of deformation in the cratonic lithosphere beneath Kimberley require pronounced weakening due to localized high water flux that can be associated with mantle metasomatism. Sheared peridotites have more depleted compositions in FeO and CaO compositions than those of granular peridotites, but have a higher orthopyroxene modal abundance and contain sodium-rich clinopyroxene, which are consistent with that extensive deformations associated with Si-rich fluid/melt metasomatism. We therefore conclude that mantle metasomatism has an important role in facilitating deformation locally within the cratonic lithosphere, and is responsible for the textural variations of peridotite xenoliths from the cratonic roots.

*Keywords*: mantle xenolith, deformation, mantle metasomatism, cratonic lithosphere

## 1. Introduction

Kimberlite pipes contain peridotite xenoliths that were derived from the deep upper mantle (70-250 km) beneath the Archean craton (e.g., Boyd, 1973). These xenoliths provide constraints on the composition, structure and thermal state of the cratonic upper mantle. The peridotite xenoliths have well developed deformation microstructures and show two textually distinct types: granular and sheared peridotites (e.g., Boyd and Nixon, 1975; Mercier and Nicolas, 1975). Coarse-grained granular peridotite is commonly considered to represent steady state mantle processes (Green and Gueguen, 1974; Harte, 1977), whereas sheared peridotite displays bimodal grain size (large porphyroclast and fine neoblast) and such transient microstructure is believed to be produced by instantaneous deformation (Green and Gueguen, 1974; Goetze, 1975; Mercier, 1979). However, the origin of the sheared peridotite still remains unclear and various models have been proposed including (1) shear heating at the lithosphere-asthenosphere boundary (Boyd and Nixon, 1975; Kennedy et al., 2002), (2) deformation driven by adiabatically rising mantle diapirs (Green and Gueguen, 1974; Gueguen and Nicolas, 1980), and (3) deformation associated by mantle metasomatism (Ehrenberg, 1979; Gurney and Harte, 1980).

The texturally distinct types of peridotite xenoliths from Lesotho are also distinguished by estimates of the *P-T* conditions, bulk composition and mineral chemistry (e.g., Harte, 1983; Boyd, 1987). The coarse granular xenoliths give *P-T* estimates of 30-45 kbar and 800-1000$^{o}$C and are characterized by highly depleted compositions. The strongly deformed shared xenoliths appear to come from deeper and

59 hotter regions ($P$ = 50-70 kbar, $T$ = 1200-1400 °C), and have relatively fertile and Fe-Ti
60 rich compositions (Boyd and Nixon, 1975). The sheared peridotites also delineate a
61 steeply rising geotherm, which is markedly different from that obtained from granular
62 xenoliths and inferred from a steady state thermal gradient (e.g., Boyd, 1973). This led
63 to the idea that the sheared peridotites originated from the lithosphere-asthenosphere
64 boundary and the steep rising geotherm is a consequence of shear heating along the
65 boundary (Boyd and Nixon, 1975). However, these data are mostly based on xenoliths
66 from the Lesotho kimberlites, and a key issue is whether these characteristics are
67 universal in the cratonic upper mantle. In this study, we analyzed mineral chemistry and
68 estimate $P$-$T$ conditions of peridotite xenoliths from Kimberley, South Africa. The
69 results indicate that not all sheared xenolith have deeper and hotter origin, and the
70 localized high water contents associated with metasomatic events are the most plausible
71 mechanism to producing the extensive deformation in the cratonic lithosphere.
72
73 **2. Sample description**
74 The Kimberley cluster of kimberlite pipes are located in central part of South Africa
75 (Fig. 1), and that is one of the type localities for Group I kimberlites. The cluster of
76 kimberlites has been dated at 84 ± 3 Ma (Clement et al., 1979). They intruded the
77 Kalahari craton, which is composed of Archean gneisses, greenstones and granitic rocks.
78 An approximately 2 km thick surface layer has been removed by erosion in the
79 Kimberley area, resulting in mid-level surface exposure of kimberlite diatremes and
80 penetration to diatreme root zones by De Beers mining activity. These exposures

provide abundant xenoliths and xenocrysts within the kimberlite magmas.

Xenoliths found in the Kimberley pipes include peridotites, eclogites, pyroxenites, glimmerites and amphibolites (Boyd and Nixon, 1978). The most abundant peridotite xenoliths are garnet harzburgites and lherzolites. We selected several garnet peridotites with less secondary alternations, including both granular and sheared type peridotites, for an analysis of mineral chemistry and equilibrium *P-T* conditions (Table 1). The granular peridotites show an equigranular texture with slightly curved grain boundaries, and consist of coarse grained (~4 mm) olivine, orthopyroxene, garnet and clinopyroxene (Fig. 2a). These peridotites contain a few recrystallized grains along the grain boundary. Crystals have almost no elongation and appear to be devoid of any foliation or lineation. The sheared peridotites show porphyroclastic texture, which contains coarse grained (~5 mm) porphyroclasts of olivine, garnet, orthopyroxene and clinopyroxene with very fine grained neoblast matrix (mostly olivine, <0.1 mm). The porphyroclasts of olivine and orthopyroxene are highly elongated and show well-developed subgrain boundaries within crystals, and a stretching lineation defined by the elongation of porphyroclasts (Fig. 2b). The modal abundances of constitute minerals in each sample are summarized in Table 2. Most samples are composed of olivine, orthopyroxene, garnet and clinopyroxene, except for one sample (Kim-22) that does not contain clinopyroxene. The sheared peridotites tend to have a higher abundance of orthopyroxene than the granular peridotites. These xenoliths display no visible evidence of extensive metasomatism, but show some secondary serpentine alteration along the grain boundary.

## 3. Mineral Chemistry

Mineral compositions were measured by electron microprobe (JEOL-JXA8200) with a wave-dispersive analyzer system at Hiroshima University. Natural silicate minerals and synthetic oxides were used as standard materials. All analyses were performed with an accelerating voltage of 15 kV, a focused electron beam current with 18 nA and a beam diameter of 3 μm. X-ray intensities were reduced using a ZAF matrix correction scheme. Representative analyses of major constitute minerals in each analyzed sample are shown in Table 3.

### *3.1. Olivine*

Olivine compositions range in Mg number (Fo content) from 90.5 to 94.5, as shown in Figure 3. There is no clear relation of the olivine Mg number and the deformation textures, but olivines in the sheared peridotites tend to have higher Mg number ($Fo_{92.5-94.4}$). Olivines are generally homogeneous in composition, and the fine-grained neoblasts have nearly identical compositions to the porphyroclasts in the sheared peridotites. NiO contents are 0.34-0.50 wt% and have a slight negative correlation with the Mg number, which is different from the depletion trend of basaltic magma. Trace element abundances such as Cr, Ca and Ti are very low, which are usually below the detection limits but some olivines contain up to 0.07 wt% $Cr_2O_3$, 0.05 wt% CaO and 0.09 wt% $TiO_2$ (Table 3).

125 *3.2. Garnet*

126 Garnets in the Kimberley peridotites are pyrope-rich ($Prp_{71-78}$) and contain moderate
127 Ca and Cr concentrations, ranging 4.3-5.9 wt% CaO and 3.5-6.0 wt% $Cr_2O_3$. Most of
128 the garnets plot within the lherzolitic field (Fig. 4), except for one sample (Kim22) that
129 has a harzbergitic garnet composition. In fact, clinopyroxene is absent in Kim22
130 although all other peridotites contain clinopyroxene and have a Ca-saturated
131 composition. The lherzolitic garnets show a positive correlation of CaO and $Cr_2O_3$ (Fig.
132 4), which is commonly observed in the other kimberlite xenoliths and is referred to the
133 lherzolite trend (Sobolev et al., 1973). The harzbergitic and lherzolitic garnets are also
134 different in Fe/Mg ratio, and the lherzolitic garnets show a positive correlation between
135 Cr content and Fe/Mg ratio (garnets in Kim46 are deviated from this trend).
136 Clinopyroxene-bearing sheared peridotites have similar garnet compositions, low
137 concentrations of Ca (4.4-4.8 wt% CaO) and Cr (3.5-4.4 wt% $Cr_2O_3$), and lower Fe/Mg
138 ratio (0.16-0.18), whereas garnets in granular peridotites show scattered chemical
139 compositions (Fig. 4). Ti and Na contents in garnets are usually low (up to 0.12 wt%
140 $TiO_2$ and 0.07 wt% $Na_2O$), but Kim46 show significantly higher concentration of $TiO_2$
141 up to 0.55 wt%. Most garnets are chemically homogeneous, but some garnet
142 porphyroclasts in sheared peridotites show a slight increase in the pyrope component
143 and a decrease in Ca content towards the rim.

144

145 *3.3. Orthopyroxene*

146 Orthopyroxenes are Mg-rich compositions ($En_{92-95}$) with trace amounts of CaO

147 (0.30-0.58 wt%), $Al_2O_3$ (0.61-1.02 wt%) and $Cr_2O_3$ (0.23-0.47 wt%). The porphyroclast
148 and neoblast orthopyroxenes in the sheared peridotites show similar composition, but
149 the neoblasts are slightly Fe-rich and contain higher CaO. In all samples, orthopyroxene
150 is more magnesium rich than the coexisting olivine, suggesting that the parageneses are
151 chemically equilibrated (Gurney et al. 1979). Ca concentrations in orthopyroxene show
152 a positive correlation with Fe/Mg ratio, and lowest Ca content is seen in Kim22, which
153 does not contain clinopyroxene (Fig. 5). However, no systematic correlation in
154 orthopyroxene compositions was observed between granular and sheared peridotites.
155 Orthopyroxenes are mostly homogeneous, but some grains show slight enrichments of
156 Ca and Al in rim domains and orthopyroxene neoblasts tend to have similar
157 compositions within porphyroclast rims.
158
159 *3.4. Clinopyroxene*
160 Clinopyroxenes have high Cr contents (1.4-2.5 wt% $Cr_2O_3$), which are classified as
161 Cr-diopside. Clinopyroxenes are separated into two groups defined by concentrations of
162 Cr and Na (Fig. 6). All sheared peridotites have clinopyroxene with high $Cr_2O_3$ (1.7-2.5
163 wt%) and $Na_2O$ (2.3-2.9 wt%). Such high Cr and Na diopsides commonly occur in
164 metasomatised peridotites in the other kimberlites (Stiefenhofer et al. 1997). Most
165 clinopyroxenes in the peridotite xenoliths have low Ti contents, less than 0.1 wt% $TiO_2$,
166 except for Kim46 in which clinopyroxene shows significantly higher concentrations of
167 $TiO_2$ (0.29-0.35 wt%). The clinopyroxene neoblasts in the sheared xenoliths have a little
168 scattered chemical composition, but are similar to the porphyroclasts (Fig. 6). Although

169 olivine and orthopyroxene show little or no compositional zoning, clinopyroxene
170 commonly exhibits significant chemical variations. This chemical zoning involves
171 increases in Na and Cr contents towards the rim and a decrease in Mg number.
172
173 **4. Pressure and temperature estimates**
174 Pressure and temperature conditions were calculated using the geothermobarometer
175 combinations of Finnerty and Boyd (1984) and Brey and Kohler (1990). In these
176 calculations, temperature estimates were based on the orthopyroxene-clinopyroxene
177 miscibility gap (Fig. 7) and pressures were estimated from the Al solubility in
178 orthopyroxene coexisted with garnet (e.g., McGregor, 1974). For the sample with no
179 clinopyroxene (Kim22), temperature was calculated using the garnet-orthopyroxene
180 Fe-Mg exchange thermometers (Harley, 1984; Brey and Kohler, 1990). Mineral
181 chemistry data used in the calculations are averages of core, rim and neoblast analyses
182 of several grains from each of the required mineral species. The results of *P-T* estimates
183 are summarized in Table 4. Most minerals are chemically homogeneous and therefore
184 give similar *P-T* conditions for the core and rim compositions. However, Kim46 shows
185 a significant pressure drop from the core to the rim, since the Al contents in
186 orthopyroxene systematically increase in the rim domains (Table 3). The chemical
187 compositions of neoblasts are a little scattered, but the averages of *P-T* estimates are
188 nearly consistent with those of the porphyroclasts.
189 The two different thermobarometer combinations yielded similar equilibration
190 temperatures and pressures: the method of Brey and Kohler (1990) shows slightly

191 higher temperatures but lower pressures (Fig. 8). The calculated *P-T* array of the
192 peridotite xenoliths agrees well with the continental geotherm with 40 $mW/m^2$ (Pollack
193 and Chapman, 1977). The Kimberley xenoliths with various textures ranging from
194 coarse granular to extremely deformed have relatively low equilibration temperatures
195 (<1130$^oC$) and appear to have originated within a limited depth interval (Fig. 8).
196 Although sheared peridotites are usually restricted to higher pressures and temperatures
197 in other kimberlites (e.g., Boyd and Nixon 1975), the equilibration temperatures and
198 pressures of the Kimberley peridotites have no systematic correlation with the
199 deformation textures.
200
201 **5. Discussion**
202 *5.1. Characteristics of the Kimberley peridotite xenoliths*
203 The garnet peridotites from Kimberley have two unique features compared to
204 xenoliths from the other kimberlites; (1) no systematic correlation between deformation
205 texture and equilibrium *P-T* conditions, and (2) depleted chemical compositions of
206 sheared peridotites. The textures of peridotite xenoliths from Lesotho show a good
207 correlation with equilibrium pressures and temperatures (e.g., Boyd and Nixon, 1975).
208 The porphyroclastic sheared peridotites tend to have a deeper origin (>170 km),
209 whereas most of coarse granular peridotites originated at shallower levels (Fig. 9). A
210 similar trend between texture and equilibrium *P-T* conditions is also found in other
211 kimberlites, including Jagersfontein, 200 km north from Kimberley (Jonston, 1973),
212 Premier, Transvaal (Danchin, 1979), Letlhakane, Botswana (Stiefenhofer et al., 1997)

213 and Jericho, northern Canada (Kopylova et al., 1999). However, the studied Kimberley
214 peridotites with various deformation textures are restricted to a relatively narrow depth
215 range (120-170 km), and there is no systematic correlation between texture and
216 estimates of equilibrium *P-T* conditions (Fig. 9). This suggests that the sheared
217 peridotites in Kimberley originate from a section of mantle that is represented by less
218 deformed rocks than most other regions. The extensively deformed peridotites in the
219 Matsoku also show relatively low temperatures and a shallower origin (Gurney et al.,
220 1975), whereas sheared peridotites in other Lesotho localities have equilibrium
221 temperatures above 1100$^{o}$C and a deeper origin. High temperature sheared peridotites
222 that are commonly found in the other kimberlites are not found in the Kimberley area.
223 However, orthopyroxene megacrysts from Kimberley appear to have higher equilibrium
224 temperatures and pressures than peridotite xenoliths (Boyd and Nixon 1978). The *P-T*
225 intervals of these megacrysts are broadly similar to those found in sheared peridotites
226 from northern Lesotho (Boyd and Nixon, 1975). The pyroxene-ilmenite intergrowth
227 texture and the deep origin of pyroxene megacrysts are considered to be indicative of a
228 crystal-mush origin within a magma chamber (Nixon and Boyd, 1973; Eggler and
229 McCallum, 1976).

230 The Kimberley peridotites have highly depleted chemical compositions. Fo contents
231 of olivine are ranging from 91 to 94 (Fig. 3), and modal abundances of clinopyroxene
232 are small, less than 4.7 vol% (Table 2). The cratonic peridotites show different chemical
233 compositional trends that are commonly found in the oceanic mantle (Boyd, 1989). The
234 Kimberley peridotite xenoliths also have distinctly chemical compositions in

235 comparison to the oceanic mantle, where olivine contents are relatively low even in
236 rocks with high olivine Mg number (Fig. 10). In the other kimberlite pipes, sheared and
237 granular peridotites show different chemical compositions; coarse granular peridotites
238 are highly depleted in FeO and CaO contents, whereas sheared peridotites are relatively
239 enriched compositions with low Mg number of olivine (Boyd, 1987). In contrast,
240 sheared peridotites in Kimberley tend to have more depleted compositions (Mg# 93-94
241 in olivine) than granular peridotites (Fig. 10), which Mg values are close to those found
242 in low-temperature granular peridotites from other kimberlites in the Kaapvaal craton
243 (Boyd, 1987). Garnet compositions of the Ca-saturated (clinopyroxene-bearing)
244 peridotites also have a tendency to show sheared peridotites that are more depleted in
245 CaO, $Cr_2O_3$ and have a higher Mg/(Mg+Fe) ratio than garnets in granular peridotites
246 (Table 3). Although olivine and garnet compositions indicate that sheared peridotites
247 have more depleted compositions than granular peridotites, clinopyroxenes in sheared
248 peridotites contain high $Na_2O$ and $Cr_2O_3$ contents (Fig. 5). Such high sodium and
249 chromium clinopyroxenes can be associated with metasomatic events as are found in
250 metasomatised lherzolites from the Letlhakane kimberlite (Stiefenhofer et al., 1997).
251 The studied Kimberley peridotites do not contain any phlogopite and amphibole, but the
252 enrichment of orthopyroxene component and the clinopyroxene compositions in sheared
253 peridotites suggest that these rocks have experienced some metasomatic events under
254 mantle conditions. Boyd (1978) reported coarse primary phlogopite in sheared xenoliths
255 from Kimberley, whereas such metasomatisms are not common in high-temperature
256 sheared peridotites in Lesotho. The silica and volatile rich metasomatisms of the

257 Kimberley peridotites are also evidenced as orthopyroxene-rich veins (Bell et al., 2005).

258

259 *5.2. Origin of the textural variation in the cratonic mantle*

260 Cratonic mantle xenoliths show distinct deformation textures, which are also
261 observed in the Kimberley peridotite xenoliths. Several mechanisms have been
262 proposed to produce the textural variations shown in the cratonic upper mantle,
263 including (1) extensive deformation at the lithosphere-asthenosphere boundary, (2)
264 deformation driven by rising mantle diapir, and (3) deformation associated with mantle
265 metasomatism. We review each model and discuss which mechanism is most plausible
266 to create the textural variations of cratonic xenoliths based on our new data.

267 Boyd (1973) recognized that the textural variations are systematically correlated
268 with equilibrium *P-T* conditions, in which sheared peridotites have a higher pressure
269 and temperature origin than coarse granular peridotites. The palaeogeotherm inferred
270 from the xenolith equilibrium conditions shows an abrupt temperature increase above
271 170 km depth where xenolith textures are dramatically changed (Boyd, 1973; Boyd and
272 Nixon, 1975). The steeply rising palaeogeotherm represented by extensively deformed
273 peridotites can not be accounted by steady state conditions, and this led to the idea that
274 the high-temperature sheared peridotites are the result of extensive deformation and
275 shear heating at the lithosphere-asthenosphere boundary (Boyd and Nixon, 1975).
276 Although this model is claimed by Goetze (1975) and Mercier (1979) that the strain
277 heating is an instantaneous process within minutes or days and the deformation
278 microstructures do not record in situ conditions in the cratonic deep mantle, Kennedy et

al. (2002) argued that a quasisteady-state shear zone exists where lithosphere and asthenosphere are partially coupled and transitory high strain-rate deformations occur heterogeneously at the boundary. However, the peridotite xenoliths from Kimberley have no systematic correlation between textures and equilibrium *P-T* conditions (Fig. 8), and the extensively deformed peridotites are restricted to a relatively shallow depths and lower temperature. This is inconsistent with the above shear-heating model in which deformations occur at greater depth at the bottom of lithosphere.

Green and Gueguen (1974) proposed an alternative mechanism where the geothermal inflection and the extensive deformation in the cratonic mantle were caused by upwelling asthenospheric mantle diapirs which may have impinged on the base of lithosphere. In this model, the chemically enriched (undepleted) and high temperature diapir was subjected to deformation at its margins as it rises trough the depleted cratonic lithosphere (Green and Gueguen, 1974). Important evidence in support of this diapir model is the correlation between textural variations and chemical compositions of peridotite xenoliths; sheared peridotites have a relatively enriched composition whereas granular peridotites are highly depleted as found in xenoliths from Lesotho (Boyd, 1987). However, this is incompatible with more depleted compositions for the Kimberley sheared peridotites (Fig. 10). The chemical compositions between sheared and granular peridotites are different in Kimberley, but these peridotites have originated from similar depths (120-160 km). This suggests that the cratonic lithosphere beneath Kimberley area has no systematic chemical stratification, but more heterogeneous chemical compositions which may be due to mantle metasomatism.

301 The final model suggests that the textural variations in cratonic mantle are
302 associated with mantle metasomatism (Ehrenberg, 1979; Gurney and Harte, 1980). The
303 similar depth origin of the extensively sheared and coarse granular peridotites at
304 Kimberley suggests large local variations of deformation. Such differences in the degree
305 of deformation might be due to hydrolytic weakening since water has a marked effect
306 on the rock strength and it can be locally distributed in the cratonic mantle as a result of
307 metasomatic fluid (or melt) infiltrations. We calculated strain-rate profile in the cratonic
308 lithosphere using grain-size piezometer (van der Wal et al., 1993) and olivine flow low
309 (Karato and Jung, 2003). The results of granular peridotites follow the steady state
310 strain-rate curve that are found in the Kaapvaal craton (Mercier, 1979), whereas sheared
311 peridotites have significant faster strain-rates and hence lower viscosity (Fig. 11). Water
312 can drastically change strain-rate of olivine-rich mantle rocks (Chopra and Paterson,
313 1984; Mei and Kohlstedt, 2000; Karato and Jung, 2003), and therefore the pronounced
314 weakening observed in the cratonic lithosphere is most likely attributed to localized
315 high water flux. Drury and van Roermund (1989) found evidence for thin fluid films
316 along grain boundaries in kimberlite xenoliths, suggesting fluid assisted
317 recrystallization in the cratonic upper mantle. Our recent analyses of dominant olivine
318 slip systems in peridotite xenoliths are also consistent with the intense deformation
319 accompanied at high water contents (Katayama et al., 2008). Although the studied
320 peridotite xenoliths have little evidence for metasomatism, sheared peridotites have high
321 abundance of orthopyroxene (Fig. 10) and sodium-rich clinopyroxenes (Fig. 6) that can
322 be associated with fluid/melt metasomatism. Kelemen et al. (1998) presents such

orthopyroxene enrichment due to interaction with $SiO_2$ rich melts produced from the subducted materials. Chemical compositions of peridotite xenoliths might be affected by the latest kimberlite intrusion. However, most mineral chemistries are considered to record in-situ mantle conditions since diffusion kinetics of major elements in crystals is much slower than the time-scale of kimberlite eruption (in hours to days). The correlation between deformation and mantle metasomatism is also supported in geochemical signatures, in which intensely deformed peridotites have enriched light rare earth elements and Sr and Nd isotopes (Dowens, 1990). We therefore conclude that mantle metasomatism plays an important role in facilitating local deformation in the cratonic lithosphere and causes the textural variations seen in peridotite xenoliths in kimberlites.

## 6. Summary

Mineral chemistries of textually variable peridotite xenoliths from Kimberley indicate that these mantle rocks were equilibrated at similar *P-T* conditions: 44-54 kbar and 970-1130$^{o}$C for granular peridotites, and 41-50 kbar and 950-1080$^{o}$C for sheared peridotites. The relatively shallow and low temperature origin of extensively deformed peridotites is a unique characteristics compared to xenoliths from other kimberlites, where sheared peridotites usually originated from deeper and higher temperature portions. The large local variations of deformation found in the Kimberley peridotites indicate that localized high water flux associated with metasomatic events likely attributed the pronounced weakening in the cratonic lithosphere. The highly depleted

FeO and CaO compositions but enriched orthopyroxene abundance and high sodium contents in clinopyroxene for sheared peridotites are also consistent with the deformation related to mantle metasomatism. These suggest that cratonic lithosphere is chemically and mechanically heterogeneous as a result of metasomatic fluid/melt infiltrations. However, such metasomatic regions should be restricted to narrow portions, otherwise it is difficult to stabilize the thick cratonic lithosphere for billions of years.

**Acknowledgements**

We thank T. Shibata for electron microprobe analysis, and K. Hirose, S. Maruyama and D. de Bruin for sample collections. Comments by A. Perchuk, T. Mitchell, and an anonymous reviewer are helpful to improve the manuscript. This study was supported by the Japan Society for the Promotion of Science.

**References**

Bell, D.R., Gregoire, M., Grove, T.L., Chatterjee, N., Carlson, R.W., Buseck, P.R., 2005. Silica and volatile-element metasomatism of Archean mantle: a xenolith-scale example from the Kaapvaal Craton. Contribution to Mineralogy and Petrology 150, 251–267.

Boyd, F.R., 1973. A pyroxene geotherm. Geochimica et Cosmochimica Acta 37, 2533-2546.

365 Boyd, F.R., 1987. High- and low-temperature garnet peridotite xenoliths and their
366 possible relation to the lithosphere-asthenosphere boundary beneath southern Africa.
367 In: Nixon, P.H. (Ed.), Mantle xenoliths. Wiley, Chichester, pp. 403-412.
368 Boyd, F.R., 1989. Compositional distinction between oceanic and cratonic lithosphere.
369 Earth and Planetary Science Letters 96, 15-26.
370 Boyd, F.R., Nixon, P.H., 1975. Origins of the ultramafic nodules from some kimberlites
371 of northern Lesotho and the Monastery mine, South Africa. Physics and Chemistry
372 of the Earth 9, 431–454.
373 Boyd, F.R., Nixon, P.H., 1978. Ultramafic nodules from the Kimberley pipes, South
374 Africa. Geochimica et Cosmochimica Acta 42, 1367-1382.
375 Brey, G.P., Kohler, T., 1990. Geothermobarometry in four-phase lherzolites II. New
376 thermobarometers, and practical assessment of existing thermobarometers. Journal
377 of Petrology 31, 1353-1378.
378 Chopra, P.N., Paterson, M.S., 1984. The role of water in the deformation of dunite.
379 Journal of Geophysical Research 89, 7861-7876.
380 Clement, C.R., Skinner, E.M., Hawthorne, J.B., Kleinjan, L., Allsopp, H.L., 1979.
381 Precambrian ultramafic dykes with kimberlite affinities in the Kimberley area. In:
382 Boyd, F.R., Meyer, H.O.A. (Eds.), Kimberlites, Diatremes and Diamonds: their
383 Geology, Petrology and Geochemistry. American Geophysical Union, pp. 101-110.
384 Danchin, R.V., 1979. Mineral and bulk chemistry of garnet lherzolite and garnet
385 harzburgite xenoliths from the Premier mine, South Africa. In: Boyd, F.R., Meyer,
386 H.O.A. (Eds.), The Mantle Sample: Inclusions in Kimberlites and Other Volcanics.

American Geophysical Union, pp. 104-126.

Downes, H., 1990. Shear zones in the upper mantle – relation between geochemical enrichment and deformation in mantle peridotites. Geology 18, 374-377.

Drury, M.R., van Roermund, H.L.M., 1989. Fluid assisted recrystallization in upper mantle peridotite xenoliths from kimberlites. Journal of Petrology 30, 133-152.

Eggler, D.H., McCallum, M.E., 1976. A geotherm from megacrysts in the Sloan kimberlite pipes, Colorado. Carnegie Institution Years Book 75, 538-541.

Ehrenberg, S.N., 1979. Garnetiferous ultramafic inclusions in minette from the Navajo volcanic field. In: Boyd, F.R., Meyer, H.O.A. (Eds.), The Mantle Sample: Inclusions in Kimberlites and Other Volcanics. American Geophysical Union, pp. 213-226.

Finnerty, A.A., Boyd, F.R., 1984. Evaluation of thermobarometers for garnet peridotites. Geochimica et Cosmochimica Acta 48, 15-27.

Goetze, C., 1975. Sheared lherzolites: from the point of view of rock mechanics. Geology 3, 172-173.

Green, H.W., Gueguen, Y., 1974. Origin of kimberlite pipes by diapiric upwelling in the upper mantle. Nature 249, 617-620.

Griffin, W.L., O'Neilly, S.Y., Natapov, L.M., Ryan, C.G., 2003. The evolution of lithospheric mantle beneath the Kalahari craton and its margins. Lithos 71, 215-241.

Gueguen, Y., Nicolas, A., 1980. Deformation of mantle rocks. Annual Review of Earth and Planetary Sciences 8, 119-144.

Gurney, J.J., Harte, B., 1980. Chemical variations in upper mantle nodules from southern Africa kimberlites. Philosophical Transactions of the Royal Society of

London A297, 273-293.

Gurney, J.J., Harte, B., Cox, K.G., 1975. Mantle xenoliths in the Matsoku kimberlite pipe. Physics and Chemistry of the Earth 9, 507-523.

Gurney, J.J., Harris, J.W., Rickard, R.S., 1979. Silicate and oxide inclusions in diamonds from the Finsch kimberlite pipe. In: Boyd, F.R., Meyer, H.O.A. (Eds.), Kimberlites, Diatremes and Diamonds: their Geology, Petrology and Geochemistry. American Geophysical Union, pp. 1-15.

Harley, S.L., 1984. An experimental study of the partitioning of Fe and Mg between garnet and orthopyroxene. Contribution to Mineralogy and Petrology 86, 359-373.

Harte, B., 1977. Rock nomenclature with particular relation to deformation and recrystallization textures in olivine-bearing xenoliths. Journal of Geology 85, 279-288.

Harte, B., 1983. Mantle peridotites and processes – The kimberlite sample. In: Hawkesworth, C.J., Norry, M.J. (Eds.), Continental Basalts and Mantle Xenoliths, Shiva, Nantwich, pp. 46-91.

Jonston, J.L., 1973. Petrology and geochemistry of ultramafic xenoliths from the Jagersfontein Mine, South Africa. Extended abstract of International Kimberlite Conference, University of Cape Town, South Africa, pp. 181-183.

Karato, S., Jung, H., 2003. Effects of pressure on high-temperature dislocation creep in olivine. Philosophical Magazine A83, 401-414.

Katayama, I., Michibayashi, K., Ando, J., Komiya, T., 2008. Distinct olivine slip systems in the granular and sheared mantle xenoliths from the Kimberley, South

Africa. Asia Oceania Geosciences Society Meeting, Busan, South Korea.

Kelemen, P.B., Hart, S.R., Bernstein, S., 1998. Silica enrichment in the continental upper mantle via melt/rock reaction. Earth and Planetary Science Letters 164, 387–406.

Kennedy, C.S., Kennedy, G.C., 1976. The equilibrium boundary between graphite and diamond. Journal of Geophysical Research 81, 2467-2470.

Kennedy, L.A., Russell, J.K., Kopylova, M.A., 2002. Mantle shear zones revisited: The connection between the cratons and mantle dynamics. Geology 30, 419-422.

Kopylova, M.G., Russell, J.K., Cookenboo, H., 1999. Petrology of peridotite and pyroxenite xenoliths from the Jericho kimberlite: Implications for the thermal state of the mantle beneath the Slave craton, Northern Canada. Journal of Petrology 40, 79-104.

Lindsley, D.H., 1983. Pyroxene thermometry. American Mineralogist 68, 477-493.

MacGregor, I.D., 1974. The system $MgO–Al_2O_3–SiO_2$: solubility of $Al_2O_3$ in enstatite for spinel and garnet peridotite compositions. American Mineralogist 59, 110–119.

Mei, S., Kohlstedt, D.L., 2000. Influence of water on plastic deformation of olivine aggregates 2. Dislocation creep regime, Journal of Geophysical Research 105, 21471-21481.

Mercier, J.C., 1979. Peridotite xenoliths and the dynamics of kimberlite intrusion. In: Boyd, F.R., Meyer, H.O.A. (Eds.), The Mantle Sample: Inclusions in Kimberlites and Other Volcanics. American Geophysical Union, pp. 197-212.

Mercier, J.C., Nicolas, A., 1975. Textures and fabrics of upper-mantle peridotites as

illustrated by xenoliths from basalts. Journal of Petrology 16, 454-487.

Nixon, P.H., Boyd, F.R., 1973. Petrogenesis of the granular and sheared ultrabasic nodule suite in kimberlites. In: Nixon, P.H. (Ed.), Lesotho kimberlites. Lesotho National Development Corporation, Maseru, pp. 48-56.

Pollack, H.N., Chapman, D.S., 1977. On the regional variation of heat flow, geotherms and lithospheric thickness. Tectonophysics 38, 279-296.

Sobolev, N.V., Lavrentev, Y.G., Pokhilenko, N.P., Usova, N.P., 1973. Cr-rich garnets from the kimberlites of Yakutia and their parageneses. Contribution to Mineralogy and Petrology 40, 39–52.

Stiefenhofer, J., Viljoen, K.S., Marsh, J.S., 1997. Petrology and geochemistry of peridotite xenoliths from the Letlhakane kimberlites, Botswana. Contribution to Mineralogy and Petrology 127, 147-158.

van der Wal, D., Chopra, P., Drury, M., Fitz Gerald, J., 1993. Relationships between dynamically recrystallized grain size and deformation conditions in experimentary deformed olivine rocks. Geophysical Research Letter 20, 1479-1482.

**Figure captions**

**Fig. 1.** Map showing the location of Kimberley as well as other major kimberlite pipes in southern Africa. The Kalahari craton is indicated by a gray field (after Griffin et al., 2003).

**Fig. 2.** Microphotographs of granular (a) and sheared (b) peridotites from Kimberley.

475 Granular peridotite has coarse-grained equigranular texture, whereas sheared peridotite
476 shows porphyroclastic texture with large porphyroclasts and very fine-grained neoblasts
477 (~0.1mm). Mineral abbreviations; Ol: olivine, Opx: orthopyroxene, Grt: garnet.
478
479 **Fig. 3.** Histograms of Mg number of olivine (Mg/(Mg+Fe) x 100) for each analyzed
480 peridotite from Kimberley. Sheared peridotites tend to have higher Mg number of
481 olivine.
482
483 **Fig. 4.** Garnet compositions of granular (open symbols) and sheared peridotites (filled
484 symbols) from Kimberley. The lherzolite and harzburgite boundary in garnet
485 composition is taken from Sobolev et al. (1973). Most garnets are plotted in the
486 lherzolite field except for one sample (Kim22), which is the clinopyroxene-free
487 peridotite.
488
489 **Fig. 5.** Orthopyroxene compositions of the Kimberley peridotites. Orthopyroxene
490 neoblasts in sheared peridotites are also plotted as gray symbol, which have similar
491 compositions to porphyroclast but slightly higher Ca content.
492
493 **Fig. 6.** Clinopyroxene compositions of the Kimberley peridotites, which are separated
494 into two groups in the $Na_2O$ and $Cr_2O_3$ contents. Clinopyroxenes in all sheared
495 peridotites have higher $Na_2O$ and $Cr_2O_3$ contents.
496

497 **Fig. 7.** Pyroxene compositions of the granular and sheared peridotites from Kimberley
498 projected onto the pyroxene four end-members; Di (Diopside), Hd (Hedenbergite), En
499 (Enstatite) and Fs (Ferrosilite). Two pyroxene solvus is shown for reference (after
500 Lindsley, 1983).
501
502 **Fig. 8.** Estimated equilibrium pressures and temperatures of the Kimberley peridotites
503 using geothermobarometer combinations of (a) Finnerty and Boyd (1984) and (b) Brey
504 and Kohler (1990). The *P-T* conditions for each peridotite are calculated from the core
505 compositions (black symbols) and rim compositions (gray symbols). The
506 diamond-graphite univariant reaction curve (Kennedy and Kennedy, 1976) and the 40
507 $mW/m^2$ continental geotherm (Pollack and Chapman, 1977) are indicated by the solid
508 lines.
509
510 **Fig. 9.** *P-T* array of the Kimberley peridotites in comparison with that of other
511 kimberlites, including Lesotho (Boyd and Nixon, 1975), Letlhakane, Botswana
512 (Stiefenhofer et al., 1997) and Jericho, north Canada (Kopylova et al., 1999), which are
513 based on the thermobarometer combinations of Finnerty and Boyd (1984). The black
514 lines/area indicate *P-T* conditions for sheared peridotites, and the gray lines/area for
515 granular peridotites. The sheared and granular peridotites from Kimberley have similar
516 *P-T* conditions and are restricted to a relatively narrow depth range, whereas sheared
517 peridotites in other localities tend to have higher temperature and pressure origins than
518 granular peridotites.

519

520 **Fig. 10.** Plot of the olivine Mg number with modal abundance of olivine for the studied
521 peridotites from Kimberley. Compiled data from the Kaapvaal craton are shown for
522 reference (Boyd, 1987). The arrow represents the compositional trend found in oceanic
523 peridotite suites (Boyd, 1989).

524

525 **Fig. 11.** Strain-rate and depth profile of the Kimberley peridotites estimated from the
526 grain-size piezometer (van der Wal et al., 1993) and the olivine flow law (Karato and
527 Jung, 2003). Granular peridotites nearly follow the steady state strain-rate curve found
528 in Kaapvaal craton (Mercier, 1979), whereas sheared peridotites have significantly
529 faster strain-rate (hence lower viscosity). Such abrupt changes of the rock strength could
530 be caused by the hydrolytic weakening due to fluid/melt metasomatism.

531

Table 1
Texture and mineral assemblage of the srudied peridotite xenoliths

| sample No. | texture | mineral assemblage |
|---|---|---|
| Kim21 | sheared type (intensely deformed) | Ol+Opx+Grt+Cpx |
| Kim22 | sheared type (intensely deformed) | Ol+Opx+Grt+Cr-Sp |
| Kim36 | granular type | Ol+Opx+Grt+Cpx |
| Kim37 | granular type (with little recrystallization) | Ol+Opx+Grt+Cpx |
| Kim46 | granular type (with little recrystallization) | Ol+Opx+Grt+Cpx |
| Kim71 | granular type | Ol+Opx+Grt+Cpx |
| Kim80 | granular type | Ol+Opx+Grt+Cpx |
| Kim91 | sheared type (intensely deformed) | Ol+Opx+Grt+Cpx |

Mineral abbreviations; Ol: olivivne, Opx: orthopyroxene, Grt: garnet,
Cpx: clinopyroxene, Cr-Sp: chromium spinel

Table 2

Modal abundances of the peridotite xenoliths (volume%)

| sample No. | Ol | Opx | Grt | Cpx |
|---|---|---|---|---|
| Kim21 | 63.7 | 31.0 | 4.7 | 0.6 |
| Kim22 | 69.8 | 26.7 | 3.5 | - |
| Kim36 | 63.9 | 29.7 | 5.8 | 0.5 |
| Kim37 | 68.1 | 28.6 | 1.9 | 1.4 |
| Kim46 | 77.4 | 18.1 | 4.3 | 0.2 |
| Kim71 | 64.9 | 22.5 | 7.9 | 4.7 |
| Kim80 | 77.2 | 15.5 | 5.1 | 2.2 |
| Kim91 | 50.6 | 42.1 | 6.6 | 0.7 |

Table 3
Representative compositions of major constituent minerals

| sample | Kim21 | | | | | | | Kim22 | | | Kim36 | | | | Kim37 | | | |
|---|---|---|---|---|---|---|---|---|---|---|---|---|---|---|---|---|---|---|
| | olivine | olivine nec | opx | opx neo | grt | cpx | cpx neo | olivine | opx | grt | olivine | opx | grt | cpx | olivine | opx | grt | cpx |
| $SiO_2$ | 40.88 | 40.95 | 57.96 | 57.92 | 42.24 | 55.05 | 55.05 | 41.29 | 57.92 | 41.82 | 40.90 | 58.12 | 41.75 | 54.83 | 41.00 | 57.94 | 41.98 | 54.62 |
| $TiO_2$ | 0.00 | 0.05 | 0.02 | 0.00 | 0.00 | 0.03 | 0.04 | 0.00 | 0.01 | 0.04 | 0.02 | 0.00 | 0.06 | 0.04 | 0.01 | 0.00 | 0.04 | 0.00 |
| $Al_2O_3$ | 0.01 | 0.02 | 0.79 | 0.81 | 20.57 | 2.92 | 2.98 | 0.00 | 0.77 | 19.83 | 0.01 | 0.73 | 20.48 | 2.91 | 0.01 | 0.74 | 19.77 | 1.65 |
| $Cr_2O_3$ | 0.02 | 0.02 | 0.32 | 0.30 | 4.12 | 2.11 | 2.17 | 0.02 | 0.46 | 5.69 | 0.02 | 0.30 | 4.34 | 2.20 | 0.02 | 0.32 | 5.33 | 1.48 |
| FeO* | 7.10 | 7.10 | 4.37 | 4.26 | 6.58 | 2.26 | 2.21 | 6.33 | 3.85 | 6.05 | 6.82 | 4.14 | 6.45 | 2.03 | 7.44 | 4.59 | 6.82 | 2.10 |
| MnO | 0.06 | 0.09 | 0.10 | 0.11 | 0.32 | 0.10 | 0.04 | 0.11 | 0.08 | 0.36 | 0.08 | 0.05 | 0.35 | 0.05 | 0.10 | 0.11 | 0.37 | 0.10 |
| MgO | 51.76 | 51.21 | 35.92 | 35.97 | 21.31 | 16.41 | 16.26 | 51.72 | 36.38 | 21.39 | 51.98 | 36.12 | 21.15 | 16.02 | 51.31 | 35.84 | 20.39 | 17.37 |
| CaO | 0.03 | 0.02 | 0.39 | 0.50 | 4.81 | 18.53 | 18.40 | 0.03 | 0.33 | 4.83 | 0.02 | 0.43 | 5.28 | 19.13 | 0.02 | 0.46 | 5.61 | 21.31 |
| $Na_2O$ | 0.00 | 0.01 | 0.12 | 0.15 | 0.04 | 2.57 | 2.52 | 0.05 | 0.11 | 0.01 | 0.00 | 0.13 | 0.00 | 2.63 | 0.00 | 0.10 | 0.02 | 1.49 |
| $K_2O$ | 0.00 | 0.00 | 0.00 | 0.00 | 0.00 | 0.01 | 0.00 | 0.01 | 0.00 | 0.01 | 0.00 | 0.01 | 0.00 | 0.00 | 0.00 | 0.00 | 0.01 | 0.02 |
| NiO | 0.45 | 0.45 | 0.00 | 0.00 | | | | 0.42 | 0.11 | | 0.41 | 0.05 | | | 0.44 | 0.08 | | |
| Total | 100.31 | 99.92 | 100.11 | 100.13 | 100.00 | 100.01 | 99.75 | 99.99 | 100.01 | 100.03 | 100.27 | 100.07 | 99.86 | 99.92 | 100.35 | 100.18 | 100.33 | 100.23 |
| | | | | | | | | | | | | | | | | | | |
| oxygen atc | 4 | 4 | 3 | 3 | 12 | 6 | 6 | 4 | 3 | 12 | 4 | 3 | 12 | 6 | 4 | 3 | 12 | 6 |
| Si | 0.985 | 0.990 | 1.981 | 1.979 | 3.009 | 1.983 | 1.986 | 0.994 | 1.975 | 2.988 | 0.985 | 1.982 | 2.986 | 1.978 | 0.989 | 1.979 | 3.003 | 1.973 |
| Ti | 0.000 | 0.001 | 0.001 | 0.000 | 0.000 | 0.001 | 0.001 | 0.000 | 0.000 | 0.002 | 0.000 | 0.000 | 0.003 | 0.001 | 0.000 | 0.000 | 0.002 | 0.000 |
| Al | 0.000 | 0.001 | 0.032 | 0.033 | 1.727 | 0.124 | 0.127 | 0.000 | 0.031 | 1.670 | 0.000 | 0.029 | 1.726 | 0.124 | 0.000 | 0.030 | 1.667 | 0.070 |
| Cr | 0.000 | 0.000 | 0.009 | 0.008 | 0.232 | 0.060 | 0.062 | 0.000 | 0.013 | 0.322 | 0.000 | 0.008 | 0.245 | 0.063 | 0.000 | 0.009 | 0.301 | 0.042 |
| Fe | 0.143 | 0.144 | 0.125 | 0.122 | 0.392 | 0.068 | 0.067 | 0.128 | 0.110 | 0.362 | 0.137 | 0.118 | 0.386 | 0.061 | 0.150 | 0.131 | 0.408 | 0.063 |
| Mn | 0.001 | 0.002 | 0.003 | 0.003 | 0.019 | 0.003 | 0.001 | 0.002 | 0.002 | 0.022 | 0.002 | 0.001 | 0.021 | 0.001 | 0.002 | 0.003 | 0.022 | 0.003 |
| Mg | 1.860 | 1.846 | 1.830 | 1.833 | 2.263 | 0.881 | 0.875 | 1.857 | 1.849 | 2.278 | 1.867 | 1.836 | 2.255 | 0.861 | 1.845 | 1.824 | 2.175 | 0.935 |
| Ca | 0.001 | 0.001 | 0.014 | 0.018 | 0.367 | 0.715 | 0.711 | 0.001 | 0.012 | 0.370 | 0.001 | 0.016 | 0.404 | 0.739 | 0.000 | 0.017 | 0.430 | 0.824 |
| Na | 0.000 | 0.000 | 0.008 | 0.010 | 0.006 | 0.179 | 0.177 | 0.002 | 0.007 | 0.002 | 0.000 | 0.009 | 0.000 | 0.184 | 0.000 | 0.006 | 0.003 | 0.104 |
| K | 0.000 | 0.000 | 0.000 | 0.000 | 0.000 | 0.000 | 0.000 | 0.000 | 0.000 | 0.001 | 0.000 | 0.000 | 0.000 | 0.000 | 0.000 | 0.000 | 0.001 | 0.001 |
| Ni | 0.009 | 0.009 | 0.000 | 0.000 | | | | 0.009 | 0.003 | | 0.009 | 0.002 | | | 0.009 | 0.003 | | |
| | | | | | | | | | | | | | | | | | | |
| Mg# | 0.929 | 0.928 | 0.936 | 0.938 | 0.852 | 0.928 | 0.929 | 0.936 | 0.944 | 0.863 | 0.931 | 0.940 | 0.854 | 0.934 | 0.925 | 0.933 | 0.842 | 0.937 |
| Ca# | | | 0.014 | 0.018 | 0.369 | 0.871 | 0.864 | | 0.012 | 0.370 | | 0.016 | 0.404 | 0.906 | | 0.017 | 0.431 | 0.920 |
| Cr# | | | 0.210 | 0.200 | 0.118 | 0.327 | 0.328 | | 0.288 | 0.161 | | 0.217 | 0.124 | 0.336 | | 0.226 | 0.153 | 0.376 |

Table 3 (continued)

| sample | Kim46 | | | | | | Kim71 | | | | Kim80 | | | | Kim91 | | | |
|---|---|---|---|---|---|---|---|---|---|---|---|---|---|---|---|---|---|---|
| | olivine | opx core | opx rim | grt core | grt rim | cpx | olivine | opx | grt | cpx | olivine | opx | grt | cpx | olivine | opx | grt | cpx |
| $SiO_2$ | 40.89 | 57.61 | 57.70 | 41.39 | 41.75 | 54.26 | 41.33 | 57.64 | 42.07 | 54.99 | 41.10 | 57.93 | 41.84 | 54.68 | 40.83 | 57.60 | 41.71 | 54.93 |
| $TiO_2$ | 0.04 | 0.11 | 0.15 | 0.52 | 0.45 | 0.35 | 0.01 | 0.01 | 0.11 | 0.12 | 0.00 | 0.00 | 0.11 | 0.11 | 0.00 | 0.04 | 0.07 | 0.09 |
| $Al_2O_3$ | 0.00 | 0.69 | 0.77 | 20.30 | 20.35 | 3.05 | 0.00 | 0.72 | 21.05 | 3.23 | 0.00 | 0.68 | 19.44 | 1.50 | 0.01 | 0.76 | 21.30 | 2.85 |
| $Cr_2O_3$ | 0.02 | 0.39 | 0.35 | 4.10 | 3.91 | 2.40 | 0.02 | 0.28 | 3.88 | 1.91 | 0.02 | 0.31 | 5.28 | 1.74 | 0.00 | 0.32 | 4.21 | 2.22 |
| FeO* | 8.72 | 4.79 | 5.05 | 7.59 | 7.66 | 2.93 | 6.52 | 4.20 | 6.21 | 2.05 | 7.22 | 4.54 | 6.99 | 1.88 | 7.34 | 4.41 | 6.75 | 2.39 |
| MnO | 0.13 | 0.13 | 0.15 | 0.32 | 0.32 | 0.04 | 0.10 | 0.09 | 0.34 | 0.09 | 0.12 | 0.08 | 0.39 | 0.09 | 0.06 | 0.08 | 0.30 | 0.08 |
| MgO | 49.79 | 35.52 | 34.88 | 20.89 | 20.83 | 16.34 | 51.67 | 35.89 | 21.75 | 15.60 | 50.92 | 35.91 | 20.19 | 17.40 | 51.54 | 35.88 | 20.92 | 16.03 |
| CaO | 0.03 | 0.57 | 0.56 | 4.85 | 4.84 | 17.25 | 0.01 | 0.41 | 4.65 | 18.64 | 0.02 | 0.39 | 5.76 | 20.97 | 0.01 | 0.36 | 4.67 | 18.65 |
| $Na_2O$ | 0.03 | 0.16 | 0.20 | 0.06 | 0.07 | 2.82 | 0.01 | 0.14 | 0.03 | 2.63 | 0.03 | 0.07 | 0.01 | 1.49 | 0.02 | 0.17 | 0.05 | 2.51 |
| $K_2O$ | 0.01 | 0.00 | 0.00 | 0.01 | 0.01 | 0.04 | 0.00 | 0.00 | 0.00 | 0.00 | 0.01 | 0.00 | 0.00 | 0.03 | 0.00 | 0.00 | 0.00 | 0.04 |
| NiO | 0.38 | 0.12 | 0.11 | | 0.00 | | 0.39 | 0.13 | | | 0.46 | 0.08 | | | 0.46 | 0.13 | | |
| Total | 100.02 | 100.08 | 99.90 | 100.05 | 100.19 | 99.55 | 100.05 | 99.51 | 100.08 | 99.29 | 99.91 | 99.98 | 100.02 | 99.97 | 100.25 | 99.76 | 99.99 | 99.85 |
| | | | | | | | | | | | | | | | | | | |
| oxygen ato | 4 | 3 | 3 | 12 | 12 | 6 | 4 | 3 | 12 | 6 | 4 | 3 | 12 | 6 | 4 | 3 | 12 | 6 |
| Si | 0.995 | 1.974 | 1.981 | 2.967 | 2.986 | 1.967 | 0.991 | 1.978 | 2.987 | 1.990 | 0.994 | 1.981 | 3.007 | 1.977 | 0.986 | 1.974 | 2.973 | 1.983 |
| Ti | 0.001 | 0.003 | 0.004 | 0.028 | 0.024 | 0.010 | 0.000 | 0.000 | 0.006 | 0.003 | 0.000 | 0.000 | 0.006 | 0.003 | 0.000 | 0.001 | 0.004 | 0.002 |
| Al | 0.000 | 0.028 | 0.031 | 1.715 | 1.716 | 0.130 | 0.000 | 0.029 | 1.761 | 0.138 | 0.000 | 0.027 | 1.646 | 0.064 | 0.000 | 0.031 | 1.789 | 0.121 |
| Cr | 0.000 | 0.010 | 0.009 | 0.232 | 0.221 | 0.069 | 0.000 | 0.008 | 0.218 | 0.055 | 0.000 | 0.008 | 0.300 | 0.050 | 0.000 | 0.009 | 0.237 | 0.063 |
| Fe | 0.178 | 0.137 | 0.145 | 0.455 | 0.458 | 0.089 | 0.131 | 0.120 | 0.369 | 0.062 | 0.146 | 0.130 | 0.420 | 0.057 | 0.148 | 0.127 | 0.402 | 0.072 |
| Mn | 0.003 | 0.004 | 0.004 | 0.019 | 0.020 | 0.001 | 0.002 | 0.003 | 0.021 | 0.003 | 0.003 | 0.002 | 0.023 | 0.003 | 0.001 | 0.002 | 0.018 | 0.002 |
| Mg | 1.807 | 1.814 | 1.785 | 2.233 | 2.221 | 0.883 | 1.847 | 1.836 | 2.302 | 0.842 | 1.837 | 1.830 | 2.163 | 0.938 | 1.855 | 1.833 | 2.223 | 0.863 |
| Ca | 0.001 | 0.021 | 0.021 | 0.373 | 0.371 | 0.670 | 0.000 | 0.015 | 0.354 | 0.723 | 0.001 | 0.014 | 0.443 | 0.812 | 0.000 | 0.013 | 0.356 | 0.721 |
| Na | 0.001 | 0.011 | 0.013 | 0.008 | 0.010 | 0.198 | 0.000 | 0.009 | 0.004 | 0.185 | 0.001 | 0.005 | 0.002 | 0.105 | 0.001 | 0.011 | 0.007 | 0.176 |
| K | 0.000 | 0.000 | 0.000 | 0.001 | 0.001 | 0.002 | 0.000 | 0.000 | 0.000 | 0.000 | 0.000 | 0.000 | 0.000 | 0.001 | 0.000 | 0.000 | 0.000 | 0.002 |
| Ni | 0.008 | 0.003 | 0.003 | | | | 0.007 | 0.004 | | | 0.010 | 0.002 | | | 0.010 | 0.004 | | |
| | | | | | | | | | | | | | | | | | | |
| Mg# | 0.911 | 0.930 | 0.925 | 0.831 | 0.829 | 0.909 | 0.934 | 0.938 | 0.862 | 0.931 | 0.926 | 0.934 | 0.837 | 0.943 | 0.926 | 0.935 | 0.847 | 0.923 |
| Ca# | | 0.021 | 0.021 | 0.376 | 0.374 | 0.835 | | 0.015 | 0.355 | 0.887 | | 0.015 | 0.444 | 0.907 | | 0.013 | 0.359 | 0.875 |
| Cr# | | 0.274 | 0.234 | 0.119 | 0.114 | 0.345 | | 0.209 | 0.110 | 0.285 | | 0.232 | 0.154 | 0.438 | | 0.218 | 0.117 | 0.343 |

*Total Fe calculated as FeO. Mg# = Mg/(Mg+Fe) atomic ratio, Ca# = Ca/(1-Na) atomic ratio, Cr# = Cr/(Cr+Al) atomic ratio.

Table 4
*P-T* estimate of the peridotite xenoliths

| | | Finnerty and Boyd (1984) | | Brey and Kohler (1990) | |
|---|---|---|---|---|---|
| | | Al in opx | cpx-opx | Al in opx | cpx-opx |
| sample | domain | *P* (kbar) | *T* (°C) | *P* (kbar) | *T* (°C) |
| Kim21 | core | 48.1 (1.2) | 1057 (14) | 45.9 (1.3) | 1120 (15) |
| | rim | 49.5 (1.7) | 1083 (21) | 45.3 (1.8) | 1113 (20) |
| | neoblast | 47.9 (2.8) | 1080 (24) | 43.7 (3.5) | 1112 (23) |
| Kim22* | core | 42.0 (1.6) | 965 (20) | 35.5 (1.6) | 927 (19) |
| | rim | 41.1 (3.0) | 953 (42) | 34.4 (2.2) | 914 (36) |
| | neoblast | 41.1 (3.8) | 952 (36) | 34.5 (3.7) | 917 (32) |
| Kim36 | core | 44.1 (1.2) | 990 (15) | 41.8 (1.5) | 1038 (19) |
| | rim | 43.6 (1.6) | 999 (21) | 41.8 (2.4) | 1055 (32) |
| Kim37 | core | 51.6 (2.3) | 1096 (38) | 37.8 (2.0) | 967 (31) |
| | rim | 53.7 (1.6) | 1132 (18) | 39.6 (1.3) | 1005 (11) |
| Kim46 | core | 53.8 (1.1) | 1124 (14) | 56.1 (2.0) | 1203 (13) |
| | rim | 51.3 (0.5) | 1098 (2) | 52.3 (1.6) | 1183 (4) |
| Kim71 | core | 46.7 (1.5) | 1020 (18) | 45.5 (1.7) | 1089 (18) |
| | rim | 46.3 (1.4) | 1031 (21) | 44.7 (1.5) | 1101 (22) |
| Kim80 | core | 44.2 (1.6) | 978 (23) | 43.0 (1.7) | 1015 (23) |
| | rim | 43.5 (1.5) | 972 (21) | 42.2 (1.4) | 1014 (20) |
| Kim91 | core | 45.6 (1.0) | 1021 (14) | 43.7 (1.3) | 1087 (17) |
| | rim | 46.2 (1.2) | 1037 (14) | 44.1 (2.0) | 1101 (17) |
| | neoblast | 44.6 (4.0) | 1035 (14) | 42.8 (4.9) | 1100 (18) |

*This sample has no clinopyroxene, and temperature was calculated using the Fe-Mg exchange between garnet and orthopyroxene (Harley 1984; Brey and Kohler 1990). Number in parenthesis is one standard deviation of the calculated pressure and temperature.

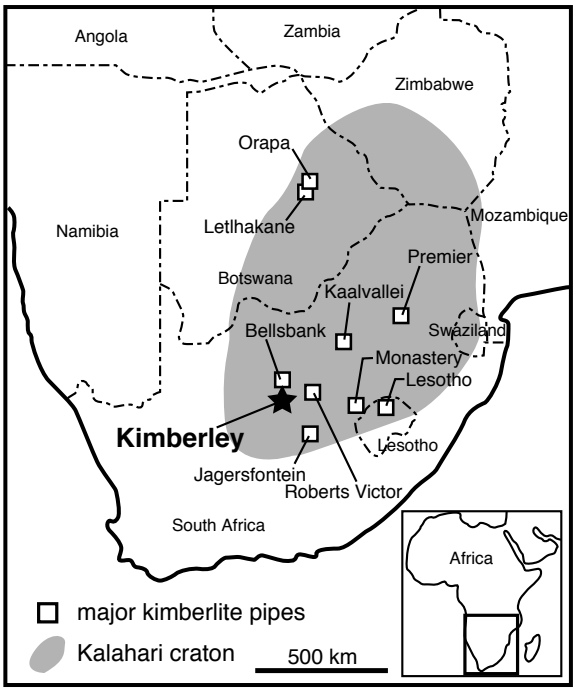


Fig. 1. Katayama et al.

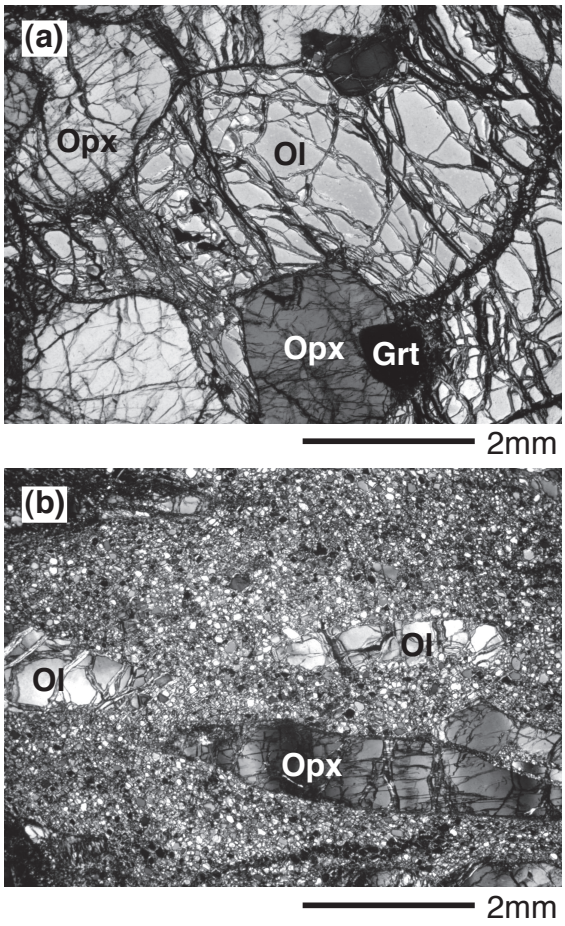


Fig. 2. Katayama et al.

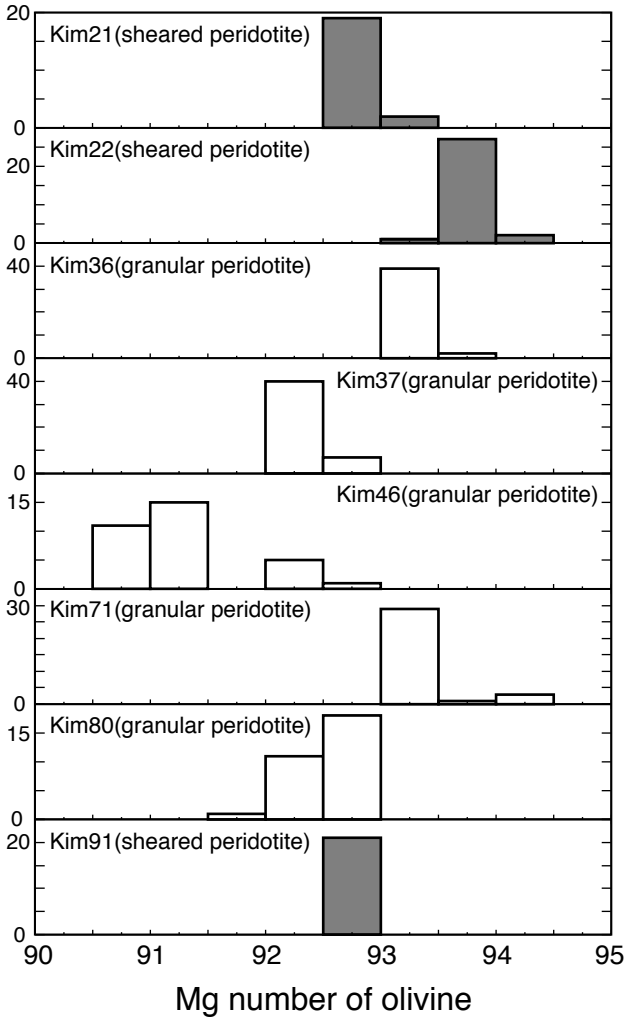


Fig. 3. Katayama et al.

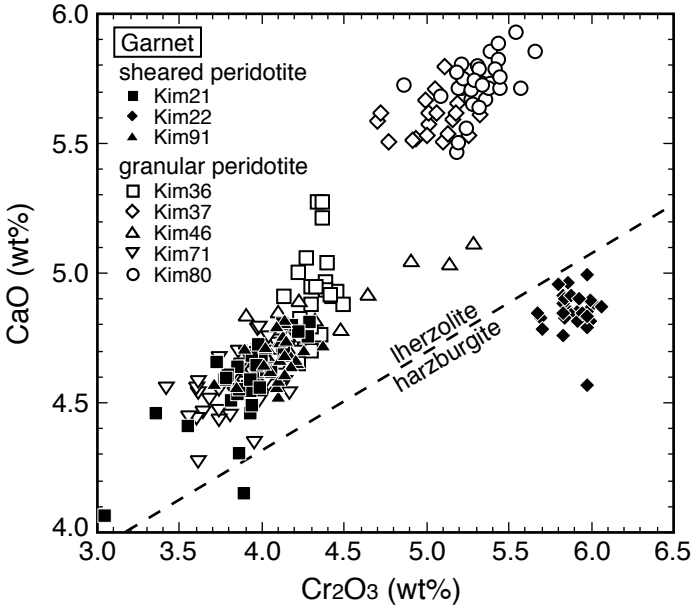


Fig. 4. Katayama et al.

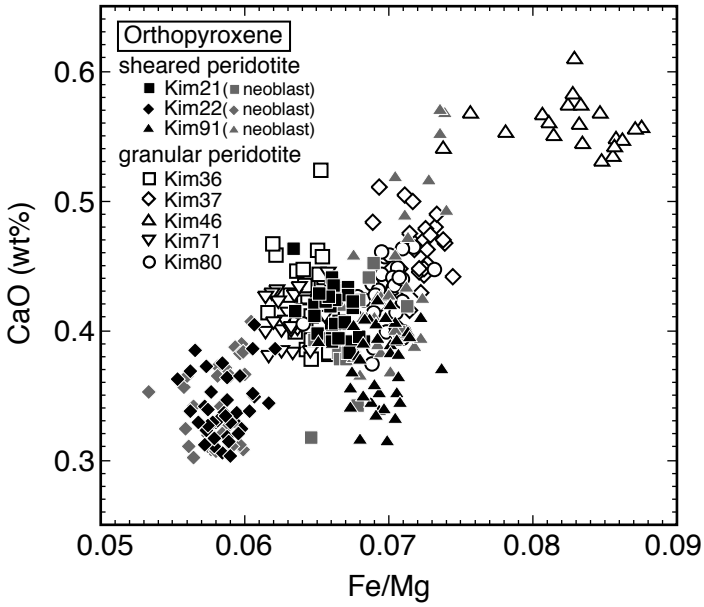


Fig. 5. Katayama et al.

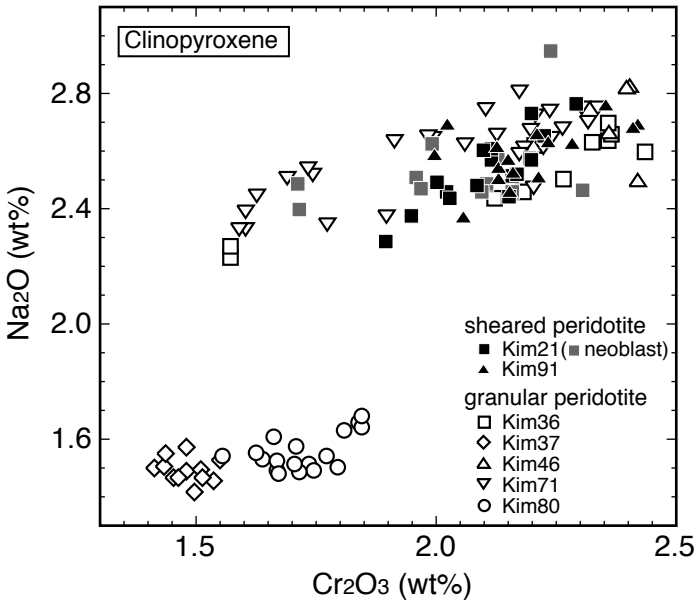


Fig. 6. Katayama et al.

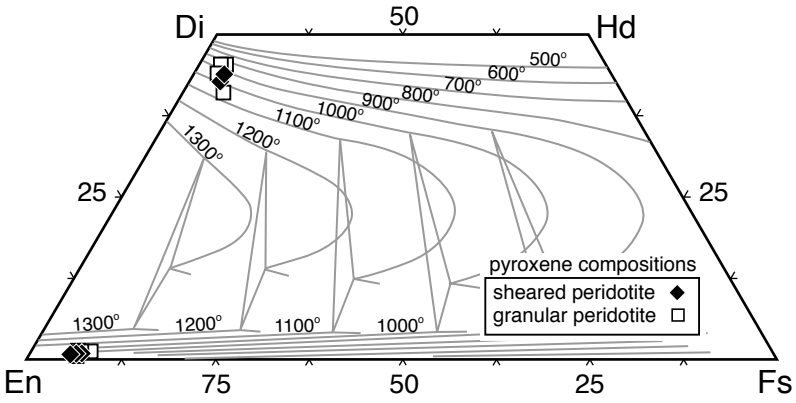


Fig. 7. Katayama et al.

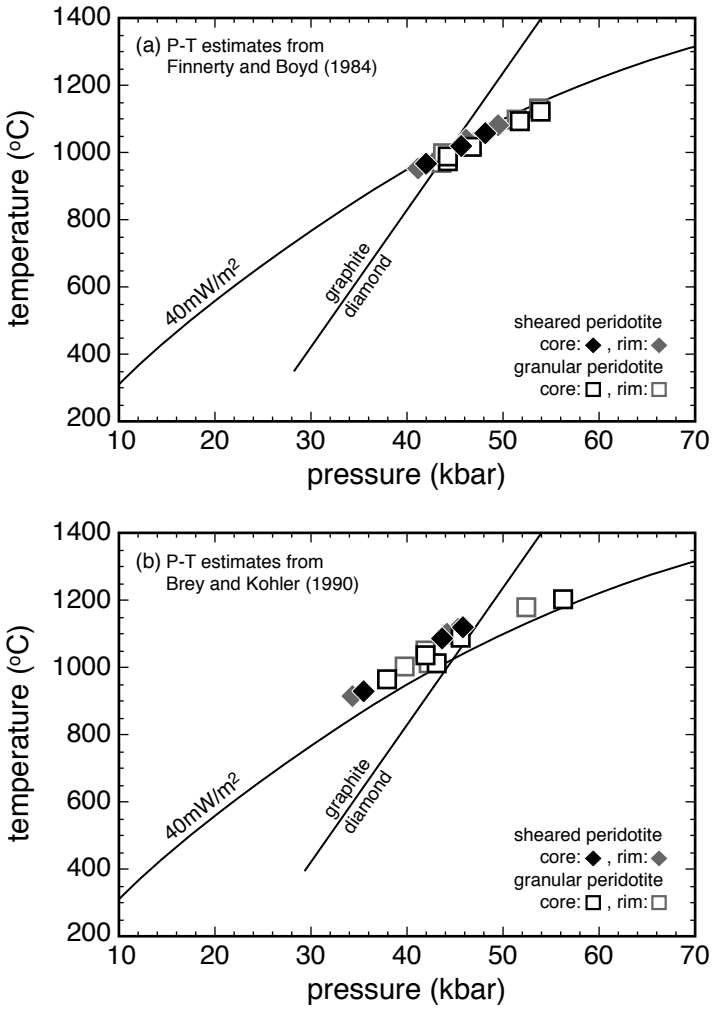


Fig. 8. Katayama et al.

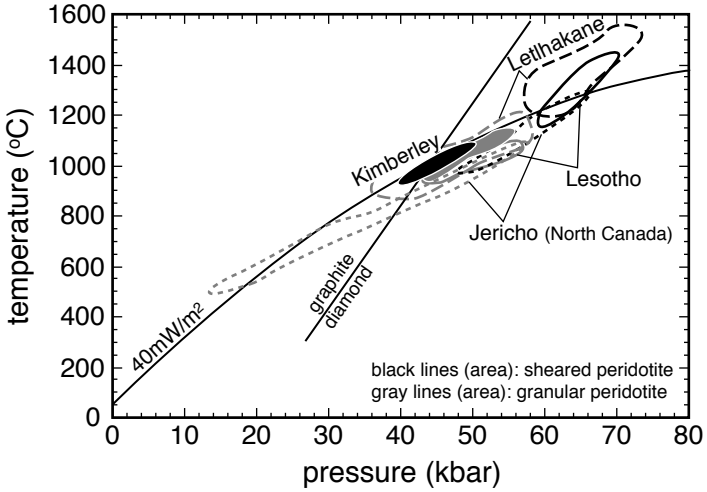


Fig. 9. Katayama et al.

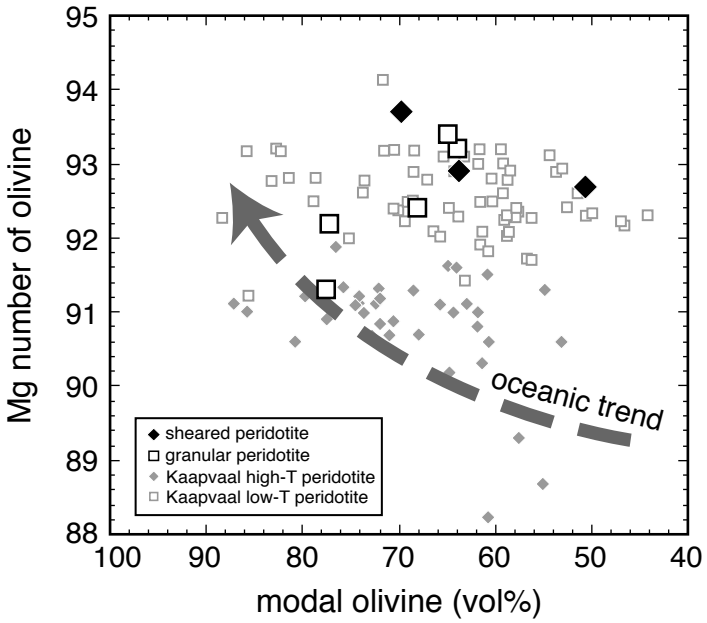


Fig. 10. Katayama et al.

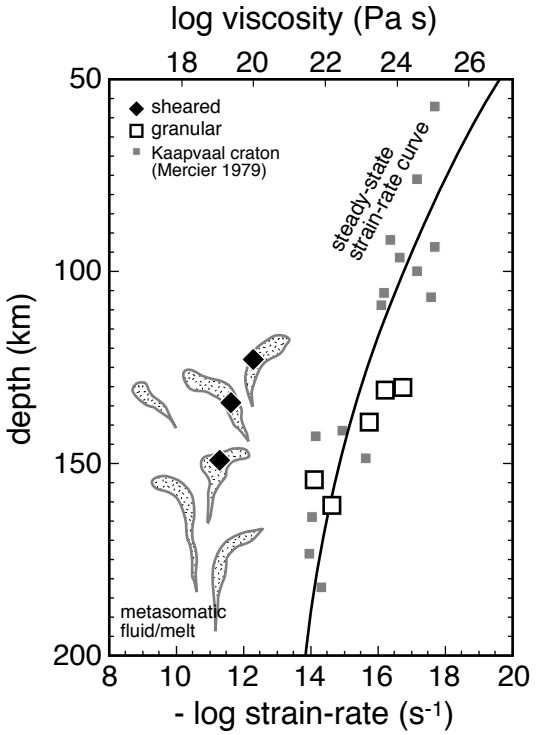


Fig. 11. Katayama et al.